JOURNAL OF COMPUTATIONAL PHYSICS 98, 181–193 (1992)

The Arctan/Tan and Kepler–Burgers Mappings for Periodic Solutions with a Shock, Front, or Internal Boundary Layer

JOHN P. BOYD

Department of Atmospheric, Oceanic, Space Science and Laboratory for Scientific Computation, 2200 Bonisteel Boulevard, Ann Arbor, Michigan 48109

Received December 28, 1989; revised October 25, 1990

Many periodic solutions have internal regions of rapid change—internal boundary layers. Shock waves and geophysical fronts are one class of examples. A second class is composed of functions which decay rapidly away from a central peak or peaks. Spherical harmonics, Mathieu eigenfunctions, prolate spheroidal wave functions, and geophysical Hough functions may all be locally approximated by Hermite functions (in the appropriate parameter range) and decay exponentially fast outside a narrow subinterval. Similarly, the large amplitude cnoidal waves of the Korteweg–DeVries equation are narrow, isolated peaks which are well approximated by the $\mathrm{sech}^2(y)$ form of the solitary wave. In this article, we show that a change-of-coordinate is a powerful tool for resolving such internal boundary layers. In the first part, we develop a general theory of mappings for the spherical harmonic/cnoidal wave class of examples, which decay rapidly away towards the edges of the spatial period. The particular map $y = \mathrm{arc\,tan}(L\,\tan(x))$ is a particularly effective choice. Four numerical examples show that this map and the Fourier pseudospectral method are a good team. In the second part, we generalize the earlier theory to describe mappings which asymptote to a constant but non-zero resolution at the ends of the periodicity interval. We explain why the "Kepler–Burgers" mapping is particularly suitable for shock and fronts.

1. INTRODUCTION

Many periodic solutions of differential equations have internal boundary layers, that is to say, regions of rapid change which are small in comparison to the interval of periodicity. A common case is that the amplitude of $u(y)$ is concentrated in a narrow region about the origin; the function is exponentially small everywhere else on $y \in [-\pi/2, \pi/2]$. One class of such examples is composed of eigensolutions to important wave equations which, in the appropriate parameter range, are accurately approximated by Hermite functions for small $|y|$ (Fig. 1a). Examples include spherical harmonics, Mathieu functions, prolate spheroidal wave equations, and Hough functions. Since the first three warrant separate chapters in the *NBS Handbook of Mathematical Functions* [1] and the Hough functions are the free modes of oscillation of the earth's atmosphere [2], it follows that such concentrated-but-periodic solutions are very important.

A second class of examples is composed of periodic generalizations of solitary waves (Fig. 1b). For the best-known case, that of water waves modelled by the Korteweg–deVries equation, these generalized solitary waves are known as "cnoidal" waves. For small amplitude, these are linear cosine waves, but for large amplitude, the cnoidal waves are flat over most of the interval except for a single narrow peak which is well approximated by the shape of the corresponding solitary wave. Thus, nonlinear wave theory also requires us to wrestle with the challenge of periodic-but-localized solutions.

Shock waves and fronts form a third class of examples. As for the Mathieu eigenfunctions and cnoidal waves, there is a region of rapid change centered on the shock. In contrast to these previous examples, however, waves with a shock usually do not decay steadily away from the region of large gradients. Instead, one needs a "high/low" change of coordinate: one that provides at least coarse resolution over the whole interval while simultaneously offering high resolution in the neighborhood of the shock.

In this work, we show that a change of coordinate of the form

$$y = f(x) \tag{1.1}$$

will convert the narrow peaks of $u(y)$ into a function $u(y[x])$ which has smooth, broad crests in x with the proper choice of the map function $f(x)$. For the concentrated-and-decaying examples, the particular transformation

$$y = \mathrm{arc\,tan}(L\,\tan(x)) \qquad \text{["Arc tan/tan map"]} \tag{1.2}$$

is extremely effective. The constant L (<1) is a map parameter that can be chosen to tune the resolution. This map has the virtues of (i) simplicity and (ii) the explicit inverse,

$$x = \mathrm{arc\,tan}([1/L]\,\tan(y)). \tag{1.3}$$

0021-9991/92 $3.00

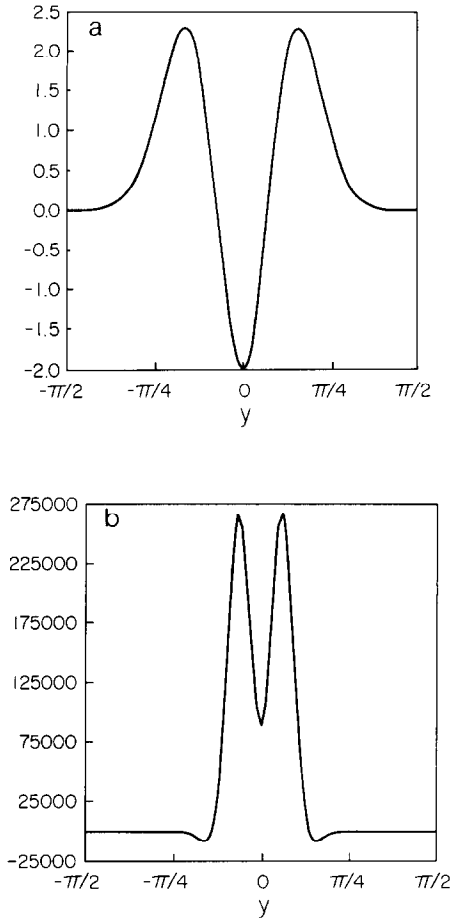

FIG. 1. Two representative examples of periodic-but-localized solutions: (a) the Mathieu function $ce_2(y)$ for $q = 2500$; (b) the bicnoidal wave of the fifth-degree Korteweg–deVries equation for $c = 100{,}000$.

First, however, we offer a brief review of how differential equations can be transformed from y to x in Section 2. The following section explains how general periodic mappings can be constructed by using the theory of "imbricate series." Section 4 is a case study which uses the general method to create a mapping based on the incomplete elliptic integral of the first kind. Section 5 shows one of the great virtues of the arc tan/tan map: When the differential equation has coefficients which are trigonometric polynomials (true of the three eigenproblems mentioned above), then a Fourier–Galerkin method in the new coordinate x will give a *banded* matrix, that is to say, a matrix in which only a small number of elements in each row is different from zero. Finally, Section 6 offers four numerical examples.

In Sections 7 and 8, we turn to shocks and fronts. The Kepler–Burgers mapping is also simple and possesses an analytic inverse. Our discussion of "high–low" mappings is more limited than that of the arc tan/tan mapping because shocks pose many difficulties. A complete treatment of shocks, comparing domain decomposition, Euler summation, and other alternatives with periodic mappings, must be left to the future. Nevertheless, the Kepler–Burgers mapping is worth an explication here.

Independently of this article and each other, Augenbaum [21, 22] and Bayliss *et al.* [23, 24] have suggested the arc tan/tan mapping in combination with a fractional linear transformation to solve *non-periodic* problems via Chebyshev polynomials. (Augenbaum [21] also treats periodic problems using a different mapping). These papers describe strategies for adaptively choosing the map parameter and, if necessary, a phase shift so as to dynamically optimize time-dependent calculations. Their adaptive tactics, not described here, could be equally well applied to periodic problems.

2. GENERAL THEORY OF MAPPING

When we make the change of coordinate

$$y = f(x), \tag{2.1}$$

where y is the original coordinate, the chain rule of elementary calculus gives

$$d/dy = (1/f'(x))\, d/dx, \tag{2.2}$$

where the prime denotes the first derivative of the mapping function. By iterating this rule, we can transform a differential or partial differential equation of arbitrary order into the corresponding equation in x. For example, consider

$$y = \text{arc tan}(L \tan(x)). \tag{2.3}$$

The chain rule gives

$$dy/dx = (2L)/[1 + L^2 + (1 - L^2)\cos(2x)]. \tag{2.4}$$

Iterating (2.4) leads to Table I.

When the solution has concentrated peaks localized every π, the map should have the form

$$y = x + V(x), \tag{2.5}$$

where $V(x)$ is periodic with a period of π. To obtain high resolution near $y = 0$ (at the price of lower resolution elsewhere), we want

$$dy/dx \ll 1 \qquad \text{near} \quad y = 0 \tag{2.6}$$

In the next section, we construct periodic maps that satisfy this constraint.

TABLE I

Expressions for y-Derivatives in Terms of x-Derivatives for the Mapping $y = \arctan(L \tan[x])$

$$u_y = Qu_x/(2L)$$

$$u_{yy} = (Q^2 u_{xx} + 2QZ \sin(2x)\, u_x)/(4L^2)$$

$$u_{yyy} = (Q/8L^3)\{Q^2 u_{xxx} + 6QZ \sin(2x)\, u_{xx} + 4Z[Z + Q\cos(2x) - Z\cos^2(2x)]\, u_x\}$$

$$u_{yyyy} = (Q/16L^4)\{Q^3 u_{xxxx} + 12ZQ^2 u_{xxx} + [28Z^2Q + 16ZQ^2\cos(2x) - 28Z^2Q\cos^2(2x)]\, u_{xx} + 8[Z^3\sin(2x) - ZQ^2\sin(2x) + 4Z^2Q\cos(2x)\sin(2x) - Z^3\cos^2(2x)\sin(2x)]\, u_x\}$$

$$u_{yyyyy} = (Q/32L^5)\{Q^4 u_{xxxxx} + 20ZQ^3\sin(2x)\, u_{xxxx} + [100Z^2Q^2 + 40ZQ^3\cos(2x) - 100Z^2Q^2\cos^2(2x)]\, u_{xxx} + 40ZQ\sin(2x)[3Z^2 - Q^2 + 6ZQ\cos(2x) - 3Z^2\cos^2(2x)]\, u_{xx} + [16Z^4 - 112Z^2Q^2 + 176Z^3Q\cos(2x) - 16ZQ^3\cos(2x) - 32Z^4\cos^2(2x) + 176Z^2Q^2\cos^2(2x) - 176Z^3Q\cos^3(2x) + 16Z^4\cos^4(2x)]\, u_x\}$$

Note. y is the original, unmapped coordinate and x is the new computational variable. L is a constant $\leqslant 1$, the "map parameter." The table uses the auxiliary parameters $Z = L^2 - 1$ and $Q(x; L) \equiv 2 + Z - Z\cos(2x)$

3. IMBRICATE SERIES AND PERIODIC CHANGES-OF-COORDINATES

To improve the resolution near $x = 0$ so that a coarse grid in the numerical coordinate x becomes a finely spaced grid in the physical coordinate y, we demand that

$$dx/dy \gg 1 \tag{3.1}$$

which is equivalent to (2.6). Thus, if we specify the mapping by setting dx/dy equal to a function $P(y)$, then this function must be sharply peaked about the origin.

If so $u(y)$ is negligibly small at the ends of the interval, that $|u(\pm\pi/2)| \ll 1$, then the solution is insensitive to approximations made at the ends of the interval. Thus, the first and simplest option for the periodic interval is to solve the problem on an *infinite* domain. The error will be the order-of-magnitude of the value of $u(y)$ at the ends of the spatial period, i.e., $O(u(\pm\pi/2))$. For the Korteweg–deVries cnoidal wave, this approach is equivalent to approximating the periodic wave by the solitary wave. The author's earlier work on infinite domain computations [3–5] can be applied without modification. The infinite interval approximation cannot be used when the boundary values are larger than the allowed error. In this situation, we must not only solve the problem on the interval $y \in [-\pi/2, \pi/2]$, but we need a mapping that is periodic so that $u(y[x])$ is periodic in x. Otherwise, the Fourier series for $u(y[x])$ would exhibit Gibbs' phenomenon and the nth Fourier coefficient would be as large as $O(u_x[\pm\pi/2]/n^2)$ [19].

At the same time, however, the periodic mapping needs to imitate the infinite interval mappings. We can reconcile these two seemingly incompatible requirements by using the theory of "imbricate series" [16, 7]. We simply define

$$dx/dy = \sum_{n=-\infty}^{\infty} P(y - n\pi), \tag{3.2}$$

where $P(y)$ is a good choice for dx/dy for an infinite interval change of coordinate. The series (3.2) converges only if $P(y)$ decays sufficiently fast as $|y| \to 0$, but all good infinite interval mappings automatically satisfy this condition. The form of the series shows that dx/dy is necessarily periodic in y with period π for *any* choice of the "pattern" function $P(y)$.

The Poisson sum formula [7, 8, 16] shows that *all* Fourier series have an alternative representation in the form of an imbricate series. Thus, we lose no generality by constructing periodic mappings in the form of (3.2).

One constraint on $P(y)$ is that it is convenient if the mapping is period-preserving, that is, the periodicity interval is π in both the physical and computational coordinates. This requires that the Fourier series for dx/dy must have the constant a_0 equal to one. The general theory of imbricate series [16, 7] shows that the Fourier coefficients are proportional to the integer values of the Fourier transform of the "pattern" function $P(y)$. This gives the simple condition

$$\int_{-\infty}^{\infty} P(y)\, dy = \pi. \tag{3.3}$$

Grosch and Orszag [10] and Boyd [3] found that for the infinite interval, *algebraic* rather than *exponential* mappings are best for general purposes. Boyd [3, 4] discusses the particular choice

$$P(y) \equiv \pi L^2/2(L^2 + y^2)^{3/2}$$

$$\leftrightarrow x = \sum_{m=-\infty}^{\infty} (\pi/2)(y - \pi m)/(L^2 + [y - \pi m]^2)^{1/2}. \tag{3.4}$$

Unfortunately, it is not possible to sum the imbricate series (3.4) in closed form nor to analytically invert the sum to obtain $y(x)$. For these reasons, we shall discuss different choices below.

It is important to note, however, that lack of an analytical sum and inverse are not fatal disqualifications. It is quite straightforward to numerically invert (3.4) or any other mapping defined by an imbricate series, since all reasonable

mappings are one-to-one and monotonic (i.e., $dx/dy > 0$). The basic step is to apply Newton's method to compute the root y of $x - g(y)$ for a given x where g is the integral of dx/dy. One begins at $x = y = 0$ and marches to larger x, using the solution at one grid point x_i to initialize the Newton's iteration at x_{i+1}.

To convert differential equations in the physical coordinate y into differential equations in x, one needs $f'(x)$ and its derivatives, the so-called "metric factors," where $y = f(x)$ is the inverse of the function specified by the imbricate series in y. Even if only $g(y)$ is known analytically, one can evaluate these metric factors via

$$f'(x) = 1/(dy/dx[y(x)] = 1/g'(y[x]) \tag{3.5}$$

and similarly for higher derivatives.

Thus, an imbricate series for $x = g(y)$ and a Newton's iteration for computing the inverse $y = f(x) = g^{-1}(x)$ are sufficient for solving differential equations in the new variable x. Nevertheless, closed form expressions for both $g(y)$ and $f(x)$ are obviously convenient, and so we shall limit the rest of the article to maps where such analytical expressions can be found.

An algebraic map similar to (3.4) is the choice

$$P(y) = A/(A^2 + y^2), \tag{3.6}$$

where

$$A(L) \equiv -\tfrac{1}{2}\log[(1-L)/(1+L)]. \tag{3.7}$$

Integration gives

$$x = \arctan([1/L]\tan(y)). \tag{3.8}$$

We omit the tedious algebra which connects (3.6) to (3.8), but note that the logarithmic singularities of (3.8) at $x = \pm iA + \pi m$, m = any integer, match in strength and location those of the imbricate series obtained by integrating (3.2) with $P(y)$ given by (3.6):

$$x = \sum_{m=-\infty}^{\infty} \arctan[(y - \pi m)/A(L)]. \tag{3.9}$$

To judge the effectiveness of this mapping, note that explicit differentiation and some rearrangement gives

$$dx/dy = (2/L)/[1 + L^{-2} + (1 - L^{-2})\cos(2y)]. \tag{3.10}$$

This shows that the resolution in the numerical coordinate x is higher than that in y by a factor of

$$\max_{\text{in } y} |dx/dy| = 1/L. \tag{3.11}$$

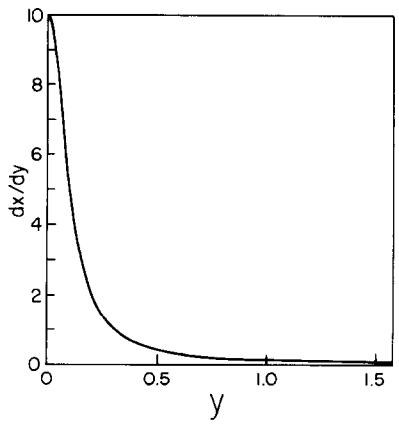

FIG. 2. Graph of dx/dy for the arc tan/tan mapping and $L = 1/10$.

The minimum resolution at $x = y = \pm\pi/2$ is

$$\min_{\text{in } y} |dx/dy| = L. \tag{3.12}$$

Figure 2 illustrates dx/dy for a particular value of the map parameter L. One can analytically and graphically analyze other maps in the same spirit.

4. THE ELLIPTIC INTEGRAL/PENDULUM MAPPING: A CASE STUDY OF THE IMBRICATE SERIES METHOD

The arc tan/tan mapping is the imbrication of a pattern function which is an *algebraic* function of y. In this section, we construct a map from a pattern function which is an *exponential* function of y:

$$P(y) \equiv \alpha\,\mathrm{sech}(sy), \tag{4.1}$$

where α and s are constants. This choice is somewhat arbitrary, but this mapping is smooth, simple, and analytically summable with an analytical inverse.

As noted earlier, theory shows that such mappings are inferior to algebraic mappings on the infinite interval [3, 4, 6, 17] in the asymptotic *limit* that the number N of spectral degrees-of-freedom tend to infinity. However, for moderate N such as $N \approx 30$, exponential transformations have been quite effective in practice [18, 20].

Noting that $\alpha = s$ to satisfy the normalization condition (3.10), it follows that

$$dx/dy = \sum_{n=-\infty}^{\infty} s\,\mathrm{sech}(s[y - n\pi]). \tag{4.2}$$

Boyd [9] has shown via Poisson summation that this imbricate series is related to the known Fourier series of an elliptic function so that

$$dx/dy = (2K(s)/\pi)\,dn(2K(s)\,y/\pi; s), \tag{4.3}$$

where $dn(u; s)$ is periodic in u with a period of $2K(s)/\pi$ where $K(s)$ is the complete elliptic integral of the first kind. (This is a minor notational change from [9] where the elliptic function had a period of unity). Integration gives [1, p. 586],

$$x = am(2Ky/\pi; s), \tag{4.4}$$

where $am(u; s)$ is the "elliptic amplitude" function. We may label this the "pendulum map" because (4.4) also describes the motion of a simple pendulum making complete revolutions about the pivot if we identify x as the polar angle θ and y as the time [15]. Its inverse is

$$y = (\pi/[2K(s)])\, F(x; k(s)) \qquad \text{["elliptic integral map"]}, \tag{4.5}$$

where $F(x; k)$ is the incomplete elliptic integral of the first kind and $k(s)$ is the usual elliptic modulus.

Boyd [9] has shown that both $K(s)$ and $k(s)$ may be computed via series that converge exponentially fast,

$$k(s) = \{\pi s/(2K[s])\} \sum_{n=-\infty}^{\infty} (-1)^n \operatorname{sech}(n\pi s), \tag{4.6}$$

where

$$K(s) = (\pi s/2) \sum_{n=-\infty}^{\infty} \operatorname{sech}(n\pi s). \tag{4.7}$$

Most special function software libraries contain routines for evaluating $F(x, k)$; in the absence of such, one can easily use the Landen transformation [1].

Thus, the elliptic integral change-of-coordinates is also simple to implement: we merely choose an appropriate s and (4.6), (4.7), and library software do the rest. However, the arc tan/tan mapping is simpler still. Furthermore, Boyd [3] and Grosch and Orszag [10] argue that mappings based on algebraic functions are usually more effective, or at least more reliable, than methods based on exponential functions (like the elliptic integral transformation) because for the latter $y(x)$ varies so rapidly near the ends of the interval that the solution is strongly singular as a function of the new coordinate x.

For these reasons, the numerical examples will be limited to the arc tan/tan mapping. Nonetheless, the construction of the elliptic integral map shows that it is easy to create periodic mappings to order for whatever special application is at hand. For the rotating pendulum [15], the elliptic integral map makes the phase angle θ a *linear* function of the transformed time. Thus, this change of coordinate would probably be useful for a *perturbed* pendulum, too.

5. BANDED GALERKIN MATRICES AND DIFFERENTIAL EQUATIONS WITH POLYNOMIAL COEFFICIENTS

One vice of pseudospectral methods is that they translate differential equations into matrix problems with dense matrices in contrast to the sparse, banded matrices created by finite difference or finite element discretizations. When the coefficients of the differential equation are trigonometric polynomials, however, it is possible to obtain a banded Fourier matrix by discretizing via Galerkin's method in place of the pseudospectral technique. Orszag and Patera [30] have been able to exploit the analogous bit of Chebyshev folklore to greatly accelerate a semi-implicit hydrodynamics code.

Unfortunately, in complicated geometries it is necessary to map the boundary into the square before applying the spectral series. The mapping introduces variable coefficients, the so-called "metric factors," into the differential equations so that constant coefficient equations in physical space become variable coefficient differential equations in the computational coordinates. Consequently, the Galerkin matrix is as dense as its pseudospectral counterpart unless the physical domain is square or rectangular.

The arc tan/tan mapping introduces "metric factors," too—they are listed for each order of derivative in Table I. In marked contrast to more general transformations, however, the arc tan/tan mapping is "polynomial-preserving": the differential equation will have polynomial coefficients in x if it had polynomial coefficients in y.

To prove this assertion, first note that differentiating the inverse map $x = \arctan([1/L]\tan(y))$ gives (3.10). Eliminating dx/dy between (3.10) and (2.4) gives

$$\cos(2y) = \{4L^2/[2 + (L^2-1)(1-\cos(2x))] - (L^2+1)\}/(L^2-1). \tag{5.1}$$

Thus, all trigonometric polynomials in y, including the metric factors in Table I, can be expressed in terms of $\cos(2x)$. This in turn implies that the Fourier–Galerkin method will yield a banded matrix for differential equations whose coefficients are trigonometric polynomials in y. Mathieu's equation, described in Section 6, is such an example.

In practice, only very simple and special differential equations have polynomial coefficients. For this reason, we will refer the reader to the author's monograph [17] for a detailed description of Galerkin's method. Exploiting polynomial coefficients is a trick rather than a general method. But sometimes it is a useful trick, and the fact that the arc tan/tan mapping is "polynomial-preserving" is therefore sometimes a virtue.

6. NUMERICAL EXAMPLES FOR THE ARC TAN/TAN MAPPING

Figure 3 illustrates the change-of-coordinate $y = \arctan[L\tan(x)]$ for three different values of L. Since $y(\pm\pi/2) = \pm\pi/2$, high resolution for small $|y|$ is inevitably counterbalanced by poorer resolution for larger $|y|$. The boundary between these two regions is the point where $dy/dx = 1$, which is

$$y_1 = \tfrac{1}{2}\arccos[(1-L)/(1+L)] \qquad \{\text{exact}\}. \quad (6.1)$$

For the appropriate range of L, we can simplify (6.1) to the following:

$$y_1 \approx \pi/4 - (1-L)/4 \qquad L \approx 1 \quad (6.2)$$

$$y_1 \approx L^{1/2} \qquad L \ll 1. \quad (6.3)$$

These expressions for $y_1(L)$ are important because, to optimize the mapping, we need to tailor the width of the region of high resolution to the width of the solution.

Optimizing L is both difficult and easy. Boyd [3] applied the method of steepest descent to optimize the map parameter L for an algebraic change of variable on an unbounded interval, but the corresponding analysis for the periodic change-of-coordinate is considerably more complex, and no simple result was obtained. Thus, a rigorous theory for optimum L is hard.

Fortunately, however, the numerical examples below demonstrate that the accuracy is not very sensitive to the precise choice of L. (Accuracy will vary smoothly with L and thus have a minimum at optimum L. Thus, a graph of accuracy versus L is flat in the neighborhood of optimum L.) Thus, the easy part of choosing L is that an educated guess of the right order-of-magnitude will be quite satisfactory. The numerical examples provide concrete guidance in choosing L for specific problems.

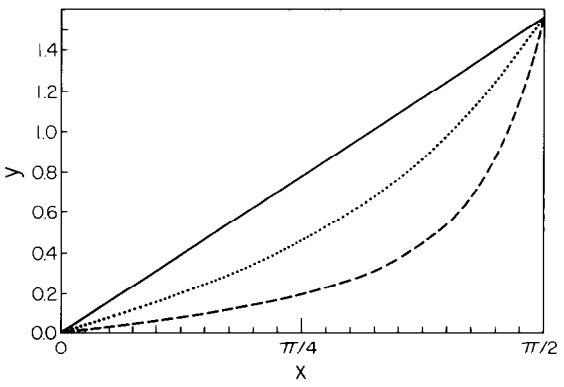

FIG. 3. The function $y = \arctan[L\tan(x)]$ for three different values of L: $L = 1$ (no mapping; solid line), $L = \frac{1}{2}$ (dotted), and $L = \frac{1}{5}$ (dashed).

Augenbaum [21, 22] and Bayliss *et al.* [23, 24] describe error-minimizing algorithms for choosing L. These are very effective in varying the mapping during a time-integration to resolve narrow, time-evolving features; we refer the reader to these articles for details and illustrations.

Because of the relative insensitivity of the error to L, however, we will adopt the more pedestrian philosophy that a good guess, combined with some simple numerical experiments, is sufficient to optimize the mapping. One set of simple experiments is to compute the expansion, for different L, of a known function which mimics the expected solution, as we shall illustrate with our first two examples below. Another set of experiments is to solve a one-dimensional shock problem with different L and a given viscosity as a prelude to computing a two-dimensional shock with the same viscosity (and therefore, a shock zone of approximately the same width).

The first two cases are the Fourier expansions of known functions constructed by choosing the pattern function $P(y)$ in the imbricate series

$$u(y) \equiv \sum_{n=-\infty}^{\infty} P(y - n\pi). \quad (6.4)$$

EXAMPLE ONE (*Dn* elliptic function; Dnoidal wave of NLS equation).

$$P(y) \equiv \operatorname{sech}(10y). \quad (6.5)$$

EXAMPLE TWO (Theta functions; periodic solutions to the heat equation; asymptotic spherical, spheroidal, & Mathieu eigenfunctions).

$$P(y) \equiv \exp(-80y^2). \quad (6.6)$$

Boyd [9] shows that all the Jacobian elliptic functions have imbricate series with hyperbolic pattern functions. In turn, the elliptic functions (or combinations and powers of elliptic functions) furnish exact periodic solutions to many nonlinear wave equations including the Korteweg–deVries equation (for which $P(y)$ is proportional to $\operatorname{sech}^2(\beta y)$ for some β) and the nonlinear Schroedinger (NLS) equation, whose periodic waves are described by the *dn* function of (6.5) and Section 4.

The Jacobian theta functions, which furnish periodic solutions to the heat equation, all have imbricate series with a Gaussian as the pattern function [14]. In addition, Mathieu's equation, Laplace's equation on the sphere, and the spheroidal wave equation all have eigenfunctions which can be approximated by imbricate series using Hermite functions as the pattern function.

Thus, these two cases, one decaying as an exponential with linear argument, the other as a Gaussian, are representative of many important applications of periodic-but-

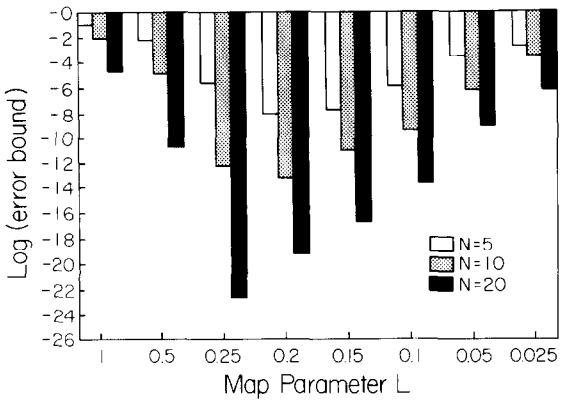

FIG. 4. Natural logarithm of the error bound as a function of the map parameter L and the truncation of the Fourier series, N, for Example One: pattern function = sech$(10y)$. (The error bound is the sum of absolute values of all the neglected coefficients, which is an upper limit on the L_∞ error.)

localized solutions in engineering and physics. Each function was expanded as an ordinary Fourier series in x [illegible] symmetric about the origin. Since the cosine functions are bounded in absolute value by 1, the error in a truncated series can be rigorously bounded by taking the sum of the absolute values of all the neglected terms. Figures 4 and 5 illustrate the results for examples one and two, respectively, for different truncations N, where $(N+1)$ is the total number of terms kept in the approximation.

The mapping is a dramatic success: in both cases, using the best value of L more than triples the number of decimal points of accuracy for all N. Furthermore, this improvement is not very sensitive to L: using L, which is 10 times smaller than the best value of L is still at least as good or better than using no change-of-coordinate at all, i.e., taking $L = 1$.

For both examples, it happens (by coincidence) that $L = \frac{1}{4}$ is a good choice (though not necessarily the best) for N between 5 and 20. Equation (6.1) shows that the high resolution region is bounded by $|y_1| = 0.46$ for this choice of map parameter. Since $\operatorname{sech}(10y_1) = 0.02$ and $\exp(-80y_1^2) = 4.5E-8$, it is obvious that for these two examples, the high resolution region must extend well beyond the "half-width" points where the pattern function has decayed to half its value at the origin.

However, there is no simple rule relating y_1 to the width of $u(y)$ such as "choose $y_1(L)$ to be well *outside* the "half-width" points. For the Mathieu eigenfunction $ce_2(y)$ (below), the half-width of the function is almost exactly equal to $\pi/4$ (see Fig. 1a). The arc tan/tan mapping is still invaluable even though for this case (and all choices of L), the region of high resolution lies *within* the half-width points.

The theta function is actually a very severe test because

$$\sum_{m=-\infty}^{\infty} \exp(-p[y-m\pi]^2) = (\pi p)^{-1/2}\left\{1+\sum_{n=1}^{\infty}\exp(-n^2/p)\cos(2ny)\right\}, \quad (6.7)$$

so that the Fourier coefficients decrease as a Gaussian in n. This is extraordinarily fast convergence; most entire functions have Fourier series that decrease as $O(\exp(-sn\log[n]))$ for some constant s while those of singular functions decrease no faster than $O(\exp(-tn))$ for some constant t [3]. The fact that the mapping still improves upon this unusually fast-converging Fourier series is remarkable.

This example also illustrates one minor vice of this change-of-coordinate: the mapping has singularities in the complex plane. This in turn implies that although $\theta(y)$ is entire, $\theta[y(x)]$ has branch points in the complex x-plane which replace the Gaussian-in-n convergence of the unmapped series (6.7) by slower geometric convergence in which the coefficients decrease as exponentials with arguments linear (as opposed to quadratic) in n. It follows that when $N \gg 1$, the optimum choice of L is one, that is, no change-of-coordinate at all. Figure 5 reflects this by showing that the best value of the map parameter increases from 0.2 for $N = 5$ to 0.5 for $N = 20$; $L_{\text{optimum}} \to 1$ (no map) in the limit $N \to \infty$.

One possible remedy is to truncate the Fourier series

$$y = \arctan[L\tan(x)] = x + \sum_{n=1}^{\infty}(-1)^n[r^n/n]\sin(2nx), \quad (6.8)$$

where

$$r \equiv (1-L)/(1+L) \quad (6.9)$$

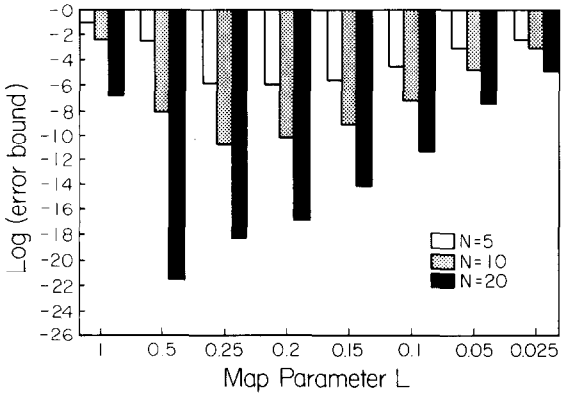

FIG. 5. Same as Fig. 4 except for Example Two: pattern function = $\exp(-80y^2)$.

after a finite number of terms, thereby generating a change-of-coordinate which is a trigonometric polynomial, free from singularities, instead of a transcendental function which has logarithmic branch points. However, we have not tested this "truncated" mapping in detail because Fig. 5 also shows that with $N=20$, the arc tan/tan map with $L=\frac{1}{2}$ still more than triples the logarithm of the error to yield nine decimal places of accuracy. At least for this example, the branch points of the map are only of academic interest.

EXAMPLE THREE (Mathieu's equation). The problem is to find $u(y)$ and λ which satisfy

$$u_{yy}+[\lambda+2q\cos(2y)]\,u=0, \tag{6.10}$$

subject to the periodic boundary conditions

$$u(y)=u(y+2\pi), \tag{6.11}$$

where λ is the eigenvalue and q is a constant. When $|q|\gg n^2$, where n is the mode number, the Mathieu functions can be approximated by Hermite functions $\psi_n(y)$. To see this, merely expand the $\cos(2y)$ in (6.10) in a power series to obtain

$$u_{yy}+[(\lambda+2q)-4qy^2]\,u=0 \tag{6.12}$$

which is the parabolic cylinder equation. The eigensolutions are then approximately

$$u_n(y)\sim\psi_n(2^{1/2}q^{1/4}y), \qquad |y|\ll 1; \qquad q\gg n^2, \tag{6.13}$$

where $\psi_n(y)$ is the nth Hermite function. Note that we have reversed the sign of q in (6.10) from what is conventional (in [1], for instance) so that the Hermite functions are centered on the origin rather than $\pi/2$; this sign reversal merely shifts the eigenfunction without altering its shape or the eigenvalue λ.

The approximation (6.13) fails at the edges of the spatial period, but this non-uniformity can be removed by generalizing (6.13) to an imbricate series with the Hermite function as the pattern function. The eigenfunctions of Mathieu's equation fall into four separate classes. Two are periodic with period π. The other two classes of eigenfunctions are periodic with period 2π and may be represented as "alternating-imbricate" series of the form

$$u(y)=\sum_{m=-\infty}^{\infty}(-1)^m\,P(y-m\pi), \tag{6.14}$$

where the pattern function is again a Hermite function.[1] For the mapping, however, the difference between (6.14) and (6.4) is meaningless: the important point is that for $|q|\gg n^2$, $u_n(y)$ has large peaks or troughs centered on $y=m\pi$ where m is an integer, and the eigenfunction has small amplitude over large subintervals between these peaks. The arc tan/tan mapping can therefore be applied to all Mathieu eigenfunctions, regardless of whether their period is π or 2π.

Figure 6 shows the results of applying the pseudospectral method to the Mathieu functions of the class which can be expanded as a sum of the even cosines: $\{1, \cos(2y), \cos(4y), \ldots\}$.

We assume

$$u(y)=\sum_{n=1}^{N+1}a_n\phi_n(y), \tag{6.15}$$

where

$$\phi_{n+1}(y)\equiv\cos(2nx[y]), \qquad n=0,\,1,\,\ldots,\,N. \tag{6.16}$$

This reduced basis—one-fourth of a *general* Fourier series—shows off another advantage of the arc tan/tan change-of-coordinate: the mapping preserves the double parity properties of the differential equation which allow this "quarter-wave" reduced basis set [17, Chap. 7].

To apply the pseudospectral method [4, 5, 7], we demand that the truncated series should exactly satisfy the differential equation at the "interpolation" or "collocation" points $y_i\equiv y(x_i)$, where

$$x_i\equiv -\pi(2i-1)/(4N+4), \qquad i=1,\,\ldots,\,N+1. \tag{6.17}$$

Note that the grid points are evenly spaced in the computational coordinate x, but the $y_i(x_i)$ are dense around $y=0$. The collocation procedure gives the matrix eigenvalue problem

$$\mathbf{Aa}=\lambda\mathbf{Ba}, \tag{6.18}$$

where $\mathbf{a}$ is the column vector whose elements are the coefficients in (6.12)

$$A_{ij}\equiv\phi_{j,yy}(y_i)+2q\cos(2y_i)\,\phi_j(y_i) \qquad i,\,j=1,\,\ldots,\,N+1 \tag{6.19a}$$

$$B_{ij}\equiv-\phi_j(y_i) \qquad i,\,j=1,\,\ldots,\,N+1, \tag{6.19b}$$

where the derivatives of the basis functions are evaluated via Table I,

$$\phi_{j,yy}(y[x])=\{Q^2[-k^2\cos(kx)]+2Q(L^2-1)\times\sin(2x)[-k\sin(kx)]\}/(4L^2), \tag{6.20}$$

where

$$Q(x;L)\equiv 2+(L^2-1)[1-\cos(2x)], \qquad k\equiv 2j-2,$$

[1] It is also possible to represent these eigenfunctions of period 2π in terms of a non-alternating imbricate series with the copies of the pattern function spaced 2π apart, but the pattern function is more complicated than (6.13), so this series is not as efficient as (6.14).

where the [ ] enclose the first and second x-derivatives of $\phi_j(y[x]) \equiv \cos(kx)$. Note that the change-of-coordinate can be buried in two subroutines: one to calculate the y_i and another which calculates the derivatives via (6.20). The main program can be written entirely in the physical coordinate y.

The QZ algorithm, available in software libraries such as the IMSL collection, will calculate the $(N+1)$ eigenvalues of (6.15) with no user input beyond the matrices **A** and **B**, but only the lowest few *matrix* eigenvalues will be good approximations to those of the *differential* equation because the higher eigenmodes oscillate too rapidly to be resolved by $(N+1)$ basis functions.

Parenthetically, note that if we applied Galerkin's method, we obtain an eigenvalue problem with a banded matrix. Unfortunately the QZ algorithm cannot exploit such bandedness, so we used the simpler and more general pseudospectral discretization instead. (There are ways to exploit bandedness in computing eigenvalues, but it would take us too far afield to discuss them here.)

Figure 6 shows the number of accurate eigenvalues for a typical case. The change-of-coordinates is clearly a godsend: five good eigenvalues when $L = 0.25$ versus only one in the absence of the mapping.

At the same time, however, Fig. 1a shows that the second mode of this class has an amplitude at $|y| = \pi/4$ which is half that at the origin. Imposing any mapping, even for L close to 1, will lower the resolution for $|y| > \pi/4$, where the eigenfunction has significant amplitude. One possible empirical rule for choosing the map parameter L would to be pick it so as to place y_1 defined by (6.1) outside the region where the mode is large, but since $y_1 \leqslant \pi/4$ for all $L \leqslant 1$, such a rule clearly fails here.

Nonetheless, Fig. 1a shows that the mode does occupy only half of the interval $y \in [-\pi/2, \pi/2]$; common sense would suggest that widening the graph of the function via the mapping would allow higher accuracy. Fig. 6 confirms this.

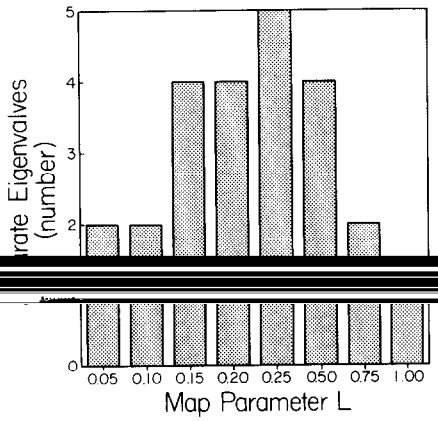

FIG. 6. The number of accurate eigenvalues for Mathieu's equation with $q = 2500$, $N = 10$, and various map parameters L. A "good" eigenvalue was arbitrarily defined to be one with an absolute error less than 30, where the average separation between eigenvalues is about 400 for this value of q.

EXAMPLE FOUR (Bicnoidal waves of the fifth-degree Korteweg–deVries (FKDV) equation). These nonlinear waves are the two-peaked, periodic solutions to

$$-u_{yyyyy} + (u - c)\, u_y = 0, \tag{6.21}$$

where c is the phase speed and $y = x - ct$ where x is the spatial coordinate. As explained in Boyd [7], solutions exist for all $c > -16.84$. To compute a solution, we begin with a first guess for a given c and then apply the Newton–Kantorovich iteration, which reduces (6.21) to the *linear* equation

$$-u^{(m+1)}_{yyyyy} + (u^{(m)} - c)\, u^{(m+1)}_y + u^{(m)}_y u^{(m+1)} = u^{(m)} u^{(m)}_y, \tag{6.22}$$

where m denotes the iteration level. Because each iteration is linear, we can apply the pseudospectral method to (6.22) with only a couple of modifications from the Mathieu case. First, the matrix problem is inhomogeneous; the column vector on the right-hand side (RHS) of the matrix equation is the RHS of (6.22), evaluated at the interpolation points. Second, the solution of (6.22) is not unique. As explained in [7], one may remove the non-uniqueness, which is caused by symmetries of the differential equation, by using a restricted basis set. Since our interest is in narrow, high amplitude solutions with $c \gg 1$, we choose to calculate in what is called the "soliton convention" [7] by using

$$\phi_n(y) \equiv (\cos[2ny] - \cos(\pi n)), \qquad n = 1, \ldots, N, \tag{6.23}$$

so that $\phi_n(\pm\pi/2) = 0$ for all n.

In the limit $c \to \infty$, the bicnoidal wave tends to the bion, the double-peaked soliton on $y \in [-\infty, \infty]$, which is a bound state of two single-crested solitons. Using the bion as computed in [7] as the pattern function for an imbricate series gave the necessary first guess for the iteration, (6.22).

Figure 1b displays $u(y)$ for the bicnoidal wave for $c = 100{,}000$. Table II shows how maximum absolute error on $y \in [-\pi/2, \pi/2]$ varies as a function of the map parameter L when the arc tan/tan mapping is used with

[redacted]

fixed N. It is also striking that any choice of map parameter $L \geqslant 0.15$ gives some improvement over no map ($L = 1$). This reiterates a theme made by the previous examples, too: the accuracy is not too sensitive to the precise value of L, and the mapping is useful even when L must be guessed.

Figure 7 shows how the accuracy varies with N for two fixed values of L. The change-of-coordinates with $L = \frac{1}{2}$

TABLE II

Maximum Absolute Error (L_∞ Error) as a Function of Map parameter L for the Bicnoidal Wave of the FKDV Equation for $c = 100{,}000$ and $N = 16$ Basis Functions

L	$\|\text{Error}\|_\infty$	$\text{Log}_{10}(\|\text{Error}\|_\infty)$
1.00	0.037	−1.43
0.75	0.000735	−3.13
0.50	0.00000224	−5.65
0.30	0.000147	−3.83
0.20	0.00244	−2.61
0.15	0.011	−1.97
0.10	0.091	−1.04

roughly doubles the number of correct decimals for all values of N.

As is characteristic of spectral methods—see similar graphs in Gottlieb and Orszag [11], for example—there is little or no accuracy until some minimum N is reached and then the error decreases exponentially fast with N. The series coefficients exhibit precisely the same behavior. Since the basis functions are bounded in absolute value by 1, one can compare numerical solutions for different L—even in the absence of a known exact solution—merely by printing out the coefficients to see which L leads to the fastest decrease. Thus, to map the parameter space of the bicnoidal wave, one would make several calculations with a different L but for a single value of c as done here. Then, once a good choice of map parameter is known, one can vary the parameter c and make many calculations with fixed L at a modest cost. Note that if the matrix problem is solved by Gaussian elimination, halving the basis set saves a factor of 8 in computer time!

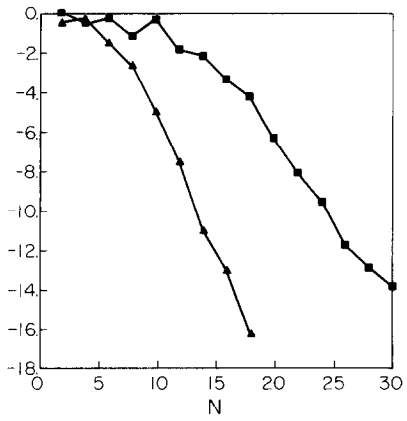

FIG. 7. The natural logarithm of the maximum of $|u(y) - u_N(y)|$ on $y \in [-\pi/2, \pi/2]$ (i.e., logarithm of the L_∞ error) is plotted versus the pseudospectral truncation N for the bicnoidal wave of the FKDV equation for $c = 100{,}000$. The upper curve (squares) is for no mapping (equivalently, $L = 1$); the lower graph (triangles) is for $L = \frac{1}{2}$.

7. "HI-LOW" CHANGES-OF-COORDINATES

The examples above all belong to the class of problems that originally motivated this work: solutions that decay exponentially fast away from a narrow peak. For such problems, it is entirely proper that dx/dy should mimic $u(y)$ by decaying rapidly to small values at the endpoints, $x = \pm\pi/2$. Poor resolution near the endpoints is acceptable because the amplitude of the solution is very small there.

Changes-of-coordinate which are applied to shocks and fronts must be different because the shock wave or geophysical flow does *not* decay away from the region of maximum gradient. With shocks, we need to resolve an $O(1)$ flow near the endpoints instead of the $O(\varepsilon)$ amplitude of the examples in Section 6.

It follows that we need to invent "hi–low" maps which give a specified high resolution around the shock or front while simultaneously retaining a lower bound on dx/dy throughout the interval. One simple tactic for defining such maps is to modify the "pattern function" $P(y)$ in (3.2) so that it converges asymptotically to a constant on the interval $y \in [-\pi/2, \pi/2]$ and then decays sufficiently fast outside this interval as $|y| \to \infty$ so that the imbricate series converges.

A simpler alternative is to modify (3.2) to

$$dx/dy = \lambda + \sum_{m=-\infty}^{\infty} P(y - m\pi; L), \tag{7.1}$$

where $\lambda < 1$ is a constant. If $P(y; L)$ decays monotonically away from $y = 0$ and if $P(\pm\pi/2) \ll \lambda$, then

$$\max |dx/dy| = \lambda + P(0), \qquad \min |dx/dy| = \lambda, \tag{7.2}$$

if $P(\pm\pi/2)$ is small enough to be neglected. Thus, we can use the extra parameter λ to control the minimum resolution, which is λ itself. The pattern function $P(y; L)$ will have an internal map parameter L which can be used to control resolution around the front, as in the earlier examples.

In this spirit, Courtier and Geleyn [25] have applied a two-dimensional mapping of the sphere to a computational sphere. Their map resolves both a small scale ("mesoscale") system and also the larger scale ("synoptic") weather systems that surround it.

8. THE KEPLER–BURGERS MAPPING FOR SHOCKS AND FRONTS

The "hi–low" mapping we shall dub the "Kepler–Burgers" change-of-coordinate is defined by

$$y = x - (t/2)\sin(2x) \qquad \text{("Kepler–Burgers" mapping).} \tag{8.1}$$

The motive for (8.1) is that many shocks and frontogenesis problems can be reduced to the inviscid Burgers' equation, also known as the "one-dimensional advection" equation,

$$u_t + uu_y = 0. \tag{8.2}$$

Its *exact* solution for the initial condition

$$u(y, t=0) = -\sin(2y)/2 \tag{8.3}$$

is given by

$$u(y, t) = -\sin[2x(y; t)]/2, \tag{8.4}$$

where $x(y; t)$ is the solution of (8.1). This algebraic equation (8.1) is known in celestial mechanics as the "Kepler" equation, so we have dubbed the mapping (8.1) as the "Kepler–Burgers" transformation.

Thus, for Burgers' equation with the sine wave initial condition, the Kepler–Burgers mapping is a kind of ultimate transformation in the sense that the Fourier solution in the computational coordinate x consists of a *single* term for all $t < 1$. For $t \geqslant 1$, the map is triple-valued; physically, the wave "breaks" and $u(y; t)$ has a jump discontinuity. No mapping can handle the post-breaking solution in the limit of zero viscosity.

However, if we generalize (8.2) by adding a dissipation term, frontogenesis will proceed until a narrow frontal zone has developed and then stop. The Kepler–Burgers mapping can resolve a slightly viscous, narrow shock zone if the parameter t is sufficiently close to 1.

In this section, we implicity assume that the coordinate y is measured in a frame of reference travelling with the wave so that the shock or front is stationary in this reference frame. As noted earlier, Augenbaum [21, 22] and Bayliss *et al.* [23, 24] have developed adaptive procedures for tracking the shock and adding a "phase shift" to the change-of-coordinates so that the region of high resolution is always centered on the shock, but we shall refer the reader to those articles for the details.

Figure 8 compares dx/dy for this map with the arc tan/tan mapping. The map parameters are chosen so that both give equal resolution at the origin, but the Kepler–Burgers transformation has much higher resolution at the ends of the interval than the arc tan/tan mapping—roughly a factor of three for $t = 0.8$. The price for this higher resolution at $y = \pm\pi/2$ is that the region of high resolution (where $dx/dy > 1$) is much narrower for the Kepler–Burgers mapping than for the arc tan/tan transformation.

In the vicinity of the origin, Taylor expansion of the sine in (8.1) gives

$$y \approx (1-t)\, x - (2/3)\, tx^3 \qquad |x| \ll 1. \tag{8.5}$$

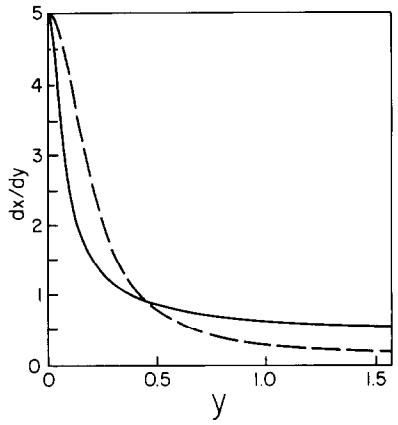

FIG. 8. Graph of dx/dy for two different types of mappings. Solid: Kepler–Burgers mapping for $t = 0.8$. Dashed: arc tan/tan mapping with $L = 0.2$. Both mappings have the same resolution (five times that of the original coordinate y) at the origin. The minimum resolution is $dx/dy = 1/(1+t) = 0.5777$ for the Kepler–Burgers mapping and $\min(dx/dy) = L = 0.2$ for the arc tan/tan transformation.

This cubic-plus-linear map was introduced for Chebyshev spectral methods by Boyd [26] and has since been rediscovered by Lacroix *et al.* [27] and Guillard and Peyret [28]. All these authors find that it resolves narrow frontal zones very well.

The Kepler equation has an analytical, infinite series solution which has been independently rediscovered at least eight times:

$$x = y - 2\sum_{n=1}^{\infty} [J_n(nt)/(nt)] \sin(2ny) \tag{8.6}$$

(Benton and Platzman [29]).

The Kepler–Burgers map could be fitted into the imbricate-plus-constant formalism of the previous section for some transcendental pattern function or other. However, the analytical form of pattern function is not known.

The Kepler–Burgers mapping can be generalized to define a whole family of transformations. If $Q(y)$ is any smooth period function, then Burgers' equation has the exact solution

$$u(y, t) = Q(x[y; t]), \tag{8.7}$$

where $x[y; t]$ is the solution of the algebraic equation

$$y = x + tQ(x). \tag{8.8}$$

Because of its simplicity, however, the Kepler–Burgers map

TABLE III

Transformation of Derivatives for the Kepler–Burgers Map
$y = x - (t/2)\sin(2x)$

$$u_y = [1/f_1(x)]\, u_x$$

$$u_{yy} = [1/f_1(x)^3]\{f_1 u_{xx} - f_2 u_x\}$$

$$u_{yyy} = [1/f_1^5]\{f_1^2 u_{xxx} - 3f_2 f_1 u_{xx} + (3f_2^2 - f_3 f_1)\, u_x\}$$

$$u_{yyyy} = [1/f_1^7]\{f_1^3 u_{xxxx} - 6f_2 f_1^2 u_{xxx} + (15f_2^2 f_1 - 4f_3 f_1^2)\, u_{xx} - (15f_2^2 - 10f_3 f_2 f_1 + f_4 f_1^2)\, u_x\}$$

Note. f_n denotes the nth derivative of the mapping function $y = f(x)$, where explicitly $f_1 = 1 - t\cos(2x)$, $f_2 = 2t\sin(2x)$, $f_3 = 4t\cos(2x)$, $f_4 = -8t\sin(2x)$, and $f_5 = -16t\sin(2x)$. Then the y-derivatives can be expressed in terms of x-derivatives as above.

is likely to be the most useful of the "Burgers transforma-

Table III lists the change-of-coordinate rules for the first five derivatives of a function. We omit numerical examples because the shock-from-a-sine-wave solution to Burgers' equation, which we used to motivate the mapping, is also an explicit illustration of the mapping's effectiveness.

9. SUMMARY

By using the method of imbricate series, we have given a general method of creating a change-of-coordinate to efficiently solve differential equations with periodic-but-localized solutions. For most purposes, the arc tan/tan mapping is sufficient: both the map and its inverse can be evaluated in terms of elementary functions, the distortion is algebraic rather than exponential as is shown to be desirable in [10], and y-derivatives can be expressed as sums of x-derivatives via Table I.

It has not been possible to offer simple rules to optimize the map parameter L; steepest descent analysis similar to Boyd [3] did not give useful results, and empirical rules based on where the resolution is raised or lowered by the mapping do not help much either. The four examples show, however, that rather modest values of L—typically 0.5 to 0.25—are best in most situations where the arc tan/tan mapping is practical. When the solution $u(y)$ fills up such a large portion of the interval $y \in [-\pi/2, \pi/2]$ that a larger L such as 0.7 is optimum, the improvement over no map ($L = 1$) will be so small that the change-of-coordinates is probably not worth the bother. On the other hand, when $u(y)$ is very, very narrowly peaked about the origin and decays exponentially away from $y = 0$, the overlap between neighboring peaks may be so small that one can ignore the periodicity and solve the problem on $y \in [-\infty, \infty]$. It is only for solutions that are narrow in comparison to the interval but not *too* narrow that the arc tan/tan mapping is useful.

Nonetheless, the examples show that such periodic-but-localized solutions are ubiquitious in solitary/cnoidal wave theory and in problems in spherical or ellipsoidal geometry. The arc tan/tan mapping and its generalization are a powerful way to improve the efficiency of Fourier pseudospectral methods for such problems.

The Kepler–Burgers mapping shows that it is also possible to develop mappings that give high resolution near the origin while maintaining a specified minimum resolution over the whole domain. The close connection between this map and Burgers' equation illustrates its potential for resolving shocks and frontal zones.

ACKNOWLEDGMENT

This work was supported by the National Science Foundation through Grants OCE8305648, OCE8509923, OCE8800123, and DMS8716766.

REFERENCES

1. M. Abramowitz and I. Stegun (Eds.), *NBS Handbook of Mathematical Functions* (Dover, New York, 1965).
2. S. Chapman and R. S. Lindzen, *Atmospheric Tides* (Gordon & Breach, New York, 1970).
3. J. P. Boyd, *J. Comput. Phys.* **45**, 43 (1982).
4. J. P. Boyd, *J. Comput. Phys.* **69**, 112 (1987).
5. J. P. Boyd, *J. Comput. Phys.* **70**, 63 (1987).
6. S. A. Orszag and M. Israeli, *Annu. Rev. Fluid Mech.* **6**, 281 (1974).
7. J. P. Boyd, *Physica D* **21**, 227 (1986).
8. P. M. Morse and H. Feshbach, *Methods of Theoretical Physics, Parts I, II* (McGraw-Hill, New York, 1953).
9. J. P. Boyd, *SIAM J. Appl. Math.* **44**, 952 (1984).
10. C. E. Grosch and S. A. Orszag, *J. Comput. Phys.* **25**, 273 (1977).
11. D. Gottlieb and S. A. Orszag, *Numerical Analysis of Spectral Methods: Theory and Applications* (Soc. Indus. Appl. Math., Philadelphia, 1977).
12. B. A. Finlayson, *The Method of Weighted Residuals and Variational Principles* (Academic Press, New York, 1972).
13. D. Gottlieb, M. Y. Hussaini, and S. A. Orszag, in *Spectral Methods for Partial Differential Equations*, edited by R. G. Voigt, D. Gottlieb, and M. Y. Hussaini (Soc. Indus. Appl. Math., Philadelphia, 1984), p. 1.
14. R. Bellman, *A Brief Introduction to Theta Functions* (Holt, Rinehart, & Winston, New York, 1961).
15. B. V. Chirikov, *Phys. Rep.* **52**, 269 (1979).
16. J. P. Boyd, in *Advances in Applied Mechanics*, Vol. 24, edited by T.-Y. Wu and J. W. Hutchinson (Academic Press, New York, 1989), p. 1.
17. J. P. Boyd, *Chebyshev and Fourier Spectral Methods* (Springer-Verlag, New York, 1989).
18. C. Canuto, M. Y. Hussaini, A. Quarteroni, and T. A. Zang, *Spectral Methods in Fluid Dynamics* (Springer-Verlag, New York, 1987).
19. J. P. Boyd, *J. Sci. Comput.* **3**, 109 (1988).
20. M. Y. Hussaini and T. A. Zang, in *Spectral Methods for Partial Differential Equations*, edited by R. G. Voigt, D. Gottlieb, and M. Y. Hussaini (Soc. Indus. Appl. Math., Philadelphia, 1984), p. 119.
21. J. M. Augenbaum, *Appl. Numer. Math.* **5**, 1 (1989).

22. J. M. Augenbaum, in *Proceedings of 2nd IMACS Symposium on Computational Acoustics, Princeton* (Elsevier–North Holland, Amsterdam, 1989).
23. A. Bayliss and B. J. Matkowsky, *J. Comput. Phys.* **71**, 147 (1987).
24. A. Bayliss, D. Gottlieb, B. J. Matkowsky, and M. Minkoff, *J. Comput. Phys.* **81**, 423 (1989).
25. P. Courtier and J.-F. Geleyn, *Q. J. Roy. Meteorol. Soc.* **114**, 1321 (1988).
26. J. P. Boyd, *J. Atmos. Sci.* **39**, 770 (1982).
27. C. Basdevant, M. Deville, P. Haldewang, J. M. Lacroix, J. Ouazzani, R. Peyret, P. Orlandi, and A. T. Patera, *Comput. Fluids* **14**, 23 (1986).
28. H. Guillard and R. Peyret, *Comput. Methods Appl. Mech. Eng.* **66**, 17 (1988).
29. E. R. Benton and G. W. Platzman, *Q. Appl. Math.* **30**, 195 (1972).
30. S. A. Orszag and A. T. Patera, *J. Fluid Mech.* **128**, 347 (1983).